PCCP

Accepted Manuscript

ROYAL SOCIETY OF CHEMISTRY

www.rsc.org/pccp

PCCP

RSCPublishing

ARTICLE

Nanoscale spinel $LiFeTiO_4$ for intercalation pseudocapacitive Li^+ storage

Cite this: DOI: 10.1039/xoxxoooooox

Ruiyong Chen,*[abc] Michael Knapp,[bc] Murat Yavuz,[bc] Shuhua Ren,[a] Ralf Witte,[ad] Ralf Heinzmann,[a] Horst Hahn,[acd] Helmut Ehrenberg[bc] and Sylvio Indris*[abc]

Received ooth January 2012,
Accepted ooth January 2012

DOI: 10.1039/xoxxoooooox

www.rsc.org/

Intercalation pseudocapacitive Li^+ storage has been recognized recently in metal oxide materials, wherein Li^+ intercalation into lattice is not solid-state diffusion-limited. This may bridge the performance gap between electrochemical capacitors and battery materials. To date, only a few materials with desired crystal structure and with well-defined nanoarchitectures have been found to exhibit such attractive behaviour. Herein, we report for the first time that nanoscale spinel $LiFeTiO_4$ as cathode material for Li-ion batteries exhibit intercalation pseudocapacitive Li^+ storage behaviour. Nanoscale $LiFeTiO_4$ nanoparticles with native carbon coating were synthesized by a sol-gel route. Fast and large-amount Li^+ storage (up to 1.6 Li^+ per formula unit over cycling) in the nanoscale $LiFeTiO_4$ host has been achieved without compromising kinetics.

1. Introduction

High-rate electrochemical energy storage systems using Li-ion batteries are desired for many practical applications. Strategies to overcome the intrinsic slow Li^+ solid-state diffusion of battery materials have focused on reducing the Li^+/e^- transport path lengths by using nanosized materials, creating fast ion-conducting surface and using nanoarchitecture materials.[1-3] Recently, a distinct Li^+ storage mechanism, intercalation pseudocapacitance, has been discovered for mesoporous Nb_2O_5 thin film.[4,5] Interestingly, the kinetics is surface-processes dependent rather than solid-state diffusion-limited. The unusual behaviour arises from enhanced Li^+ ions adsorption at/migration through interconnected sheets of NbO_x faces in the bulk Nb_2O_5, as revealed by ab initio molecular dynamics simulations.[6] Li^+ are accommodated in quasi-two-dimensional planes in the van der Waals gaps of the host lattice. This finding is distinct from the traditional concepts of (1) charge storage with the formation of electric double-layer, and (2) redox pseudocapacitive charge storage (Faradaic reactions) only at the surface/near-surface of materials.[7-9] The significance of this discovery is that Li^+ storage in battery materials can be achieved at short timescales comparable to that for electrochemical capacitors. However, Li^+ storage through intercalation pseudocapacitance mechanism is rarely observed in most intercalation materials. So far, only a few metal oxides such as orthorhombic Nb_2O_5,[5] α-MoO_3[10] and monoclinic TiO_2[11] with open channels in crystal structure and well-defined nanoarchitectures in material morphology (such as iso-oriented crystalline walls, ordered mesoporous thin film, nonorods with facile Li^+ diffusion path through the across-section) show such attractive behaviour. Besides, Li^+ storage in these oxide (anode) materials is restricted to low operation voltage (< 3.2 V).

Among various intercalation hosts of Li-ion battery materials, spinel-type framework structures have received particular attention as Li^+ hosts allowing three dimensional (3D) pathways for fast Li^+ diffusion with low energy barrier.[12] Nanoscale materials with increased accessible surface area to electrolytes often exhibit enhanced redox pseudocapacitive contribution for charge storage occurring at the surface of particles.[13] The effect of particle size (15–210 nm) on the Li^+ storage properties of spinel $LiMn_2O_4$ has been studied systematically.[14] Nanosized particles are capable of accommodating Li^+ with expanded solid-solution limits. The combination of spinel crystal structure and nanoscale materials has been demonstrated as a feasible way for high-rate Li^+ storage.[14,15] By comparing previous works on the capacitive Li^+ storage for spinel anode $Li_4Ti_5O_{12}$,[15,16] it is speculated that the crystallite size plays a more important role for exhibiting enhanced pseudocapacitive Li^+ storage rather than the mesoporous thin film structure. Hence, downsizing the particles to a few nanometers is important to explore the distinct material properties.

Herein, nanoscale spinel $LiFeTiO_4$ was synthesized through a sol-gel route. This material is used as a model intercalation cathode material for Li-ion batteries to study the Li^+ storage mechanism. It has been found that $LiFeTiO_4$ may form spinel solid-solution with $Li_4Ti_5O_{12}$.[17] Furthermore, lithiation induced

lattice changes in $Li_4Ti_5O_{12}$-$LiFeTiO_4$ solid-solution have been assumed to be similar to that for pure $Li_4Ti_5O_{12}$. Lithiation of bulk spinel $LiFeTiO_4$ may result in the full Fe^{3+}/Fe^{2+} reductions at a flat plateau of ~2.3 V without changes in lattice structure.[18] Thus, the $LiFeTiO_4$ fulfills the requisite for intercalation pseudocapacitance with excellent structural stability and minor lattice changes.[5] In addition, electrochemical delithiation with partial Fe^{3+}/Fe^{4+} oxidation for $LiFeTiO_4$ may occur, as observed in tunnel structure $LiFeTiO_4$ ($CaFe_2O_4$ structure, space group *Pnma*).[19] Beyond one-electron reaction per transition metal in intercalation cathodes is also of great interest for obtaining higher capacity. Surprisingly, the nanoscale $LiFeTiO_4$ shows superior Li^+ storage performance of high-capacity (a maximum of 1.6 Li^+ capacity over cycling) and excellent rate-capability. Electrochemical/structural characterization reveals that Li^+ storage proceeds with slight changes in lattice parameters, and the Li^+ storage kinetics is not solid-state diffusion-limited. We demonstrate for the first time nanoscale spinel material, synthesized by a general solution route, exhibited intercalation pseudocapacitance phenomenon for Li^+ storage.

2. Experimental

$LiFeTiO_4$ nanoparticles with native carbon coating were synthesized by a sol-gel route followed by thermal sintering. Polyvinylpyrrolidone (PVP, 1 300 000) used as carbon source was added into a mixture of isopropanol and propionic acid. Afterwards, Li_2CO_3 (5% Li-excess), $Fe(NO_3)_2{\cdot}9H_2O$ and $Ti[OCH(CH_3)_2]_4$ were added into the solution described above under vigorous stirring. After evaporating the solvents, the xerogels were dried under vacuum at 90 °C for 8 h and sintered subsequently at 600 °C (5 °C min^{-1}) for 4 h under flowing Ar. The final $LiFeTiO_4$/C composite consisted of 17 wt% carbon, as measured by a catalytic combustion method (vario macro, Elementar).

Electrochemical tests were performed using a Swagelok cell using lithium as anode, $LiPF_6$ as Li^+ electrolyte (1 M in 1:1 (v/v) ethylene carbonate/dimethyl carbonate) and glass fibers as separator. The working electrodes were prepared by grinding the as-obtained $LiFeTiO_4$/C powders and carbon black at a weight ratio of 4:1. The charge-discharge performance was evaluated between 1.5–4.8 V (and also up to 5 V) versus lithium at 40 °C and at room temperature at different current rates from 0.05C to 1C. For *ex situ* structural analysis of the cycled materials, the Swagelok cells were disassembled in a glovebox and the electrode was rinsed with dimethyl carbonate and then dried at room temperature.

Powder X-ray diffraction (XRD) patterns were recorded on a STOE diffractometer using Mo-Kα_1 radiation (λ = 0.7093 Å). Rietveld structure refinements were performed using FullProf.[20] For synchrotron pair distribution function (PDF) analysis, total scattering data were collected at Petra-III beamline P02.1 (λ = 0.2068 Å) at DESY in Hamburg, Germany. Raw data processing and structural fitting were described elsewhere.[21] *Ex situ* room temperature ^{57}Fe Mössbauer spectra were acquired using ^{57}Co (Rh) as γ-ray source in transmission geometry. The velocity scale was calibrated with metallic α-Fe foil. ^{7}Li magic-angle spinning (MAS) nuclear magnetic resonance (NMR) spectroscopy experiments were performed on a Bruker Avance 200 MHz spectrometer (B_0 = 4.7 T) using a 1.3 mm zirconia rotor and a sample rotation frequency of 60 kHz at 25 °C with a rotor-synchronized Hahn-echo pulse sequence ($\pi/2$-τ–π-τ acquisition).[21] Spectra were referenced to a 1 M LiCl solution at 0 ppm. TEM images were recorded with a Titan 80-300, FEI microscope.

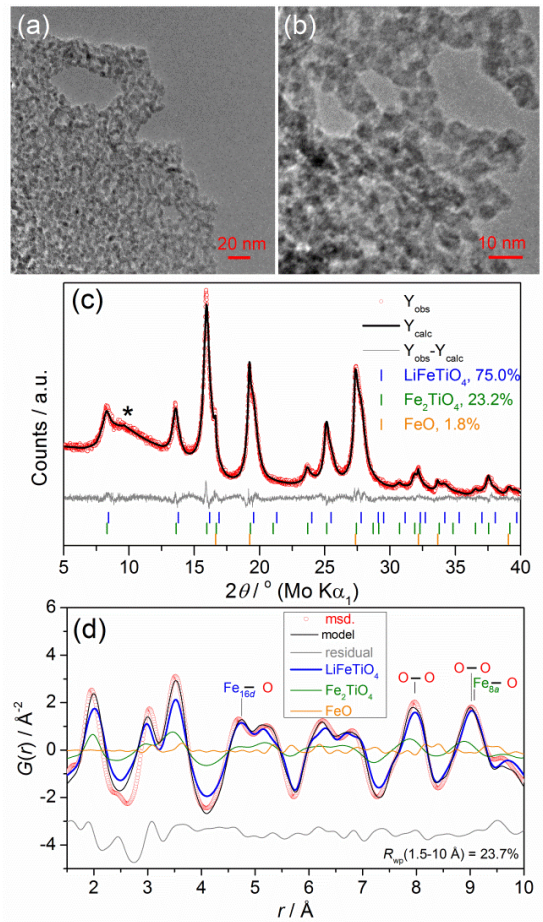

Fig. 1 Characterizations of as-prepared $LiFeTiO_4$/C. (a,b) TEM images. (c) XRD pattern and Rietveld refinement. The asterisk marks the diffraction peak from native graphite. (d) Experimental and calculated atomic PDF profiles.

3. Results and discussion

3.1. Pristine materials. To obtain nanosized $LiFeTiO_4$, PVP was added into the initial sol solutions and which decomposes into carbon matrix surrounding the $LiFeTiO_4$ phase after post-sintering. The crystal growth/agglomeration of $LiFeTiO_4$ can be inhibited effectively.[22] Fig. 1a,b shows the TEM images of the $LiFeTiO_4$ nanoparticles with a size less than 5 nm, a fairly uniform size distribution and well-dispersed character. XRD Rietveld analysis yields a cubic spinel structure $LiFeTiO_4$ (75 wt%, space group *Fd*-3*m*, *a* = 8.354 Å)[17,23,24] and a refined crystallite size of about 3 nm (Fig. 1c, Table S1). Two impurity

phases (spinel Fe_2TiO_4,[25] rock-salt FeO) have been found in the as-prepared materials. The presence of Fe^{2+} impurities is related to the reductive environment during the post-sintering of the sol-gel products. These Fe^{2+} species are found to be inert upon charging (oxidation), as confirmed by Mössbauer spectroscopy. A strong 220 reflection peak at $2\theta = 13.61^o$ suggests the partial occupancy of tetrahedral 8*a* sites by Fe^{3+} in spinel $LiFeTiO_4$.[17,24] In addition, the refinement suggests that the interstitial octahedral 16*c* sites are partially occupied by Fe^{3+} (~12%). This is different from the previous reports.[23,24,26] For micrometer-sized particles, the long-range Li^+ transport in the *Fd*-3*m* symmetry can be hampered due to blocking of the Li^+ transport through 8*a*→16*c*→8*a* path.[26,27] However, for the present nanoscale $LiFeTiO_4$, the Li^+ kinetics are found to be not restricted by the Fe_{Li} site-defects.

Atomic PDF analysis, performed using the structure mode derived from Rietveld refinement, may provide better structure determination for nanophase materials than diffraction methods.[28] Except for the low-*r* region (< 3 Å), the model shows a good fit (Fig. 1d). The refined Fe_{8a}–O and Fe_{16d}–O distances of the first coordination shells are 1.92(5) and 2.06(1) Å, respectively.[26] In addition, the PDF shows decay of the intensity at ~50 Å (as will be discussed below), suggesting the coherent domain size of about 5 nm. Thus, different techniques (TEM, XRD Rietveld refinement, PDF) confirmed the nanocrystalline character of the as-prepared materials. The combination of spinel crystal structure and nanophase materials is expected to exhibit fast Li^+ storage performance.

3.2. Electrochemical Li^+ storage performance. The $LiFeTiO_4$ materials were cycled against lithium anode between 1.5–4.8 V at varied current rates (Fig. 2a,b). Higher charging voltages up to 5 V were also applied in order to examine the possible Fe^{3+}/Fe^{4+} oxidation (Fig. 2c,d). The oxidative decomposition of $LiPF_6$ electrolyte occurs when charging to 5 V.[29] Accordingly, the coulombic efficiency decreases slightly from 99.9% (when charging to 4.8 V) to ~96% (when charging to 5 V) (Fig. 2d). The charge curves show slope profile and a short plateau is present above ~4.5 V. The discharge curves show slope profiles below 3.5 V. Different discharge features can be observed when using different charging cutoff voltages. The capacity contribution above ~2.4 V increases when charging to higher voltages (Fig. 2a,c). Note that a flat charge/discharge plateau at about 2.3 V has been observed for $LiFeTiO_4$ synthesized by a solid-state reaction when cycling between 1–3 V corresponding to Fe^{3+}/Fe^{2+} redox couple.[18] Thus, for the nanoscale $LiFeTiO_4$, higher discharge voltage might be related to the partial formation of Fe^{4+} upon charging and the slope charge/discharge profile is associated with the single phase intercalation reaction and enhanced capacitive Li^+ storage, as will be discussed below. Over cycling, $LiFeTiO_4$ exhibits reversible Li^+ storage behaviour and progressively increased capacity. A maximal discharge capacity of 250 mAh g^{-1} (i.e., ~1.6 Li^+ per formula unit) has been observed after 150 cycles at 0.05C rate (Fig. 2b), which is higher than that expected for a one-electron Fe^{3+}/Fe^{2+} reaction (154 mAh g^{-1}).[24] The origin of the extended capacity for $LiFeTiO_4$ may arise from (1) a full one-electron Fe^{3+}/Fe^{2+} reaction, (2) a possible partial Fe^{4+}/Fe^{3+} reaction, (3) a partial Ti^{4+}/Ti^{3+} reaction (from $LiFeTiO_4$ and Fe_2TiO_4 impurity) when cycling below 2 V, (4) enhanced surface redox charge storage due to nanosized character. The redox reactions of Fe, Ti and the Li^+ storage mechanism will be discussed below. Good capacity retention at high rates was also observed for $LiFeTiO_4$ (Fig. 2b). $LiFeTiO_4$ shows a reversible discharge capacity of ~90 mAh g^{-1} at a 4C rate and 40°C over 300 cycles (Fig. S1).

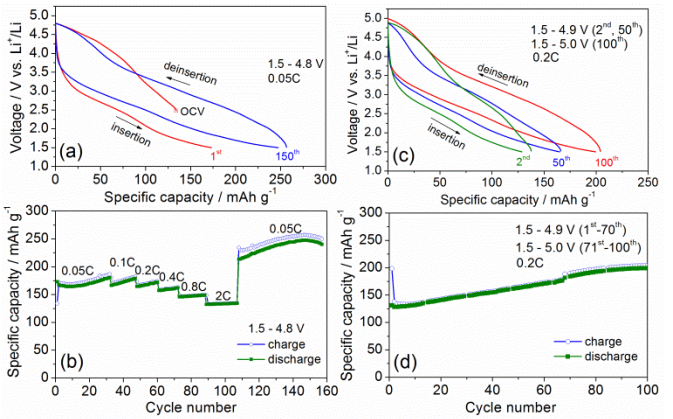

Fig. 2 Charge-discharge profiles and cycling stability of $LiFeTiO_4$/C tested at 40°C between (a,b) 1.5–4.8 V and (c,d) 1.5–4.9 V during the first 70 cycles and then 1.5–5.0 V. 1C corresponds to 154 mA g^{-1} assuming a one-electron reaction.

3.3. Li^+ kinetics characterization. CV curves in Fig. 3a,b show broad redox peaks and the cathodic reduction reactions are centered at 3.1 and 2.6 V. $LiFeTiO_4$ shows enhanced oxidation current response above 4.5 V, which might be related to tetrahedral Fe^{3+} oxidation.[22,30] The discharge voltage at 3.1 V becomes evident after 50 cycles and the integrated area of CV curves becomes larger over cycling. Ti^{4+}/Ti^{3+} redox couple occurs slightly close to the cutoff voltage (~1.7 V).[17,31,32] The kinetic characterizations were studied by performing CV experiments with varied scan rates ranging from 0.05 to 1 mV s^{-1} (corresponding to charging/discharging timescales between ~18 and 0.9 h). Faster sweep rates were not used due to larger ohmic contribution.[5] As a function of scan rate (υ), the CV current response (i) arising from the solid-state diffusion-controlled intercalation reactions ($i_{dc} = k_1\upsilon^{0.5}$) and from the interface-related pseudocapacitive contribution ($i_{pc} = k_2\upsilon$) can be well distinguished.[5,33] Fig. 3b depicts the normalized current (i/υ, i.e., capacitance) versus potential for different scan rates. The striking similarity of the superimposed curves confirms that the Li^+ storage arises mainly from capacitive contribution. Fig. 3c shows linear relationship between two cathodic peak currents and scan rates, indicating a typical pseudocapacitive behaviour. Low cathodic peak voltage offset (< 0.1 V) was also observed by increasing scan rates. Furthermore, the overall current response at a given voltage in the CV curves, arising from the diffusion and capacitive contributions, can be separated using the equation, $i(V) = k_1\upsilon^{0.5} + k_2\upsilon$.[34] The shaded

region in Fig. 3d shows the significant pseudocapacitive contribution to the total Li^+ storage.

Note that the timescales for CV measurements are comparable to that for the galvanostatic charge/discharge tests (from 0.05C to 1C) in Fig. 2. Thus, the superior Li^+ storage capability of $LiFeTiO_4$ observed in Fig. 2 is associated with the capacitive charge storage. Further structural studies of the $LiFeTiO_4$ over cycling confirm a typical intercalation reaction with minor crystal structure changes, which will be discussed below. These results indicate that the Li^+ storage in the nanoscale $LiFeTiO_4$ through an intercalation pseudocapacitance process.

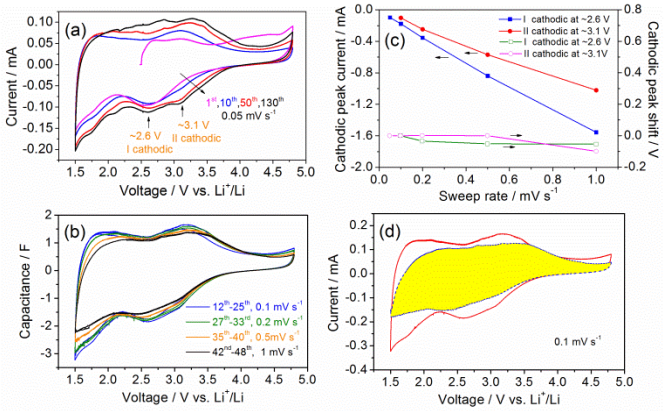

Fig. 3 (a) CV curves for $LiFeTiO_4$ measured between 1.5–4.8 V at 40 °C. (b) Potential-dependent capacitance calculated from CV responses at different sweep rates. (c) Cathodic peak current and peak voltage offset versus sweep rate for labeled reduction peaks in (a). (d) CV at a sweep rate of 0.1 mV s^{-1} shows the capacitive contribution (shaded region) to the total current.

3.4. ^{57}Fe Mössbauer spectra. ^{57}Fe Mössbauer spectrum of as-prepared material in Fig. 4a show two Fe^{3+} doublets with isomer shifts (IS) of 0.32 and 0.35 mm s^{-1} (Table S2), corresponding to initial Fe^{3+} ions in $LiFeTiO_4$. The Fe^{3+} distribution over the tetrahedral and octahedral sites in $LiFeTiO_4$ cannot be well resolved due to the strong overlapping of the subspectra.[23] Two Fe^{2+} doublets were observed for the as-prepared material, which arise from the Fe^{2+}-containing impurities as observed from XRD. The Fe^{3+}:Fe^{2+} ratio derived from the XRD phase analysis (65:35) matches well with the one from Mössbauer spectroscopy. The quantified amounts of Fe^{2+}-species remain unchanged after first charge (Fig. 4b) and also after 160th charge (Fig. 4c), suggesting that the Fe^{2+}-species in the pristine material are electrochemically inactive.

After charging to 4.8 V, the Mössbauer spectrum shows a pronounced shift from about 0.3 mm s^{-1} towards lower velocity values (Fig. 4b,c), implying the decrease of the number of the d-electrons at Fe nuclei.[35] The fitted IS values (IS = 0.19, 0.16, 0.04 mm s^{-1}, Table S2) after charging are close to those reported previously for tetragonal Fe^{4+},[22,30,36] but larger than that expected for typical octahedral Fe^{4+} ion (negative IS).[35,37] Note that Fe^{4+} species formed during charge may oxidize the electrolyte, leading to Fe^{3+} species.[38] Thus, techniques with *in situ* observation of Fe^{4+} should provide accurate and reliable quantification. In addition, Fe^{4+} ions show large voltage hysteresis during discharge.[30,39,40] Thus, Fe^{4+}/Fe^{3+} reduction reaction cannot be well defined from the discharge curves and CV measurements. On charging, Li^+ extraction out of $Li_{1-y}Fe^{3+\delta}TiO_4$ has been confirmed by ^{7}Li NMR (discussed below). In this work, we assign tentatively the iron species with IS values of 0.04–0.19 mm s^{-1} as $Fe^{3+\delta}$.[35] In the fully discharged state Fe species can be largely reduced to Fe^{2+} (93%, Fig. 4d), indicating that around one Li^+ can be inserted into the $Li_{1+y}FeTiO_4$ (y = 0.93) host. The Mössbauer spectra confirm the reversible full Fe^{3+}/Fe^{2+} couple reactions over cycling.

The bulk redox reaction of Fe indicates the Li^+ storage in the crystal lattice. This is the typical character for intercalation electrodes. These above-discussed results confirm that nanoscale $LiFeTiO_4$ exhibits features of pseudocapacitive materials despite the Li^+ storage occurring in the material bulk. This is consistent with the intercalation pseudocapacitance Li^+ storage mechanism.[5]

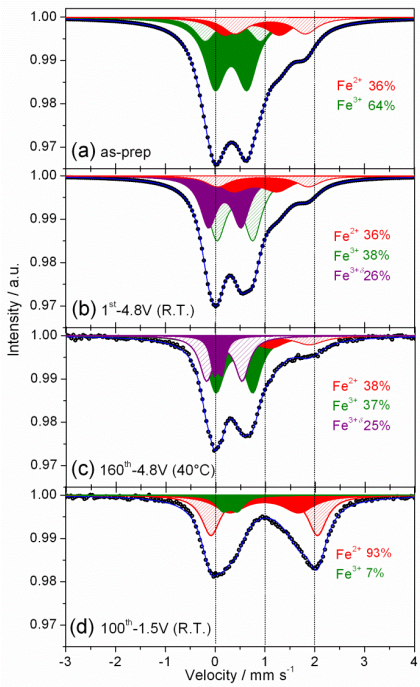

Fig. 4 ^{57}Fe Mössbauer spectra of as-prepared and cycled $LiFeTiO_4$/C. The deconvoluted spectra are shown as coloured lines for the identified iron doublets.

3.5. XRD, ^{7}Li NMR and PDF analysis. Insertion of about one Li^+ into the spinel $LiFeTiO_4$ will lead to $Li_{1.93}FeTiO_4$, as revealed from electrochemical and Mössbauer data. On discharging to 1.5 V, there is no noticeable change in the XRD pattern (Fig. S2). Similarities were reported for spinel $Li_{1.2}Fe_{0.4}Ti_{1.4}O_4$[17] and $Li_{1.3}Fe_{0.1}Ti_{1.6}O_4$[31]. The insertion of Li^+ into these spinel phases causes only the changes in the relative intensities of the diffraction peaks and slight shifts of the peak positions. It is assumed that upon lithiation the phase evolution

behaviour of $LiFeTiO_4$ is analogous to that observed for $Li_4Ti_5O_{12}$.[41,42] Furthermore, we confirmed that the crystal structure of the electrochemically generated $Li_{1.93}FeTiO_4$ is different from that of chemically prepared Li_2FeTiO_4 (*Fm*-3*m*).[43,44] In addition, the lithiation voltage for the spinel $LiFeTiO_4$ is about 0.2 V higher than that for the chemically synthesized rock-salt Li_2FeTiO_4 (~2.4 V).[43] These results indicate a small effect of Li^+ insertion/extraction on the spinel host framework and thus a single-phase and quasi zero-strain lithiation/delithiation behaviour.

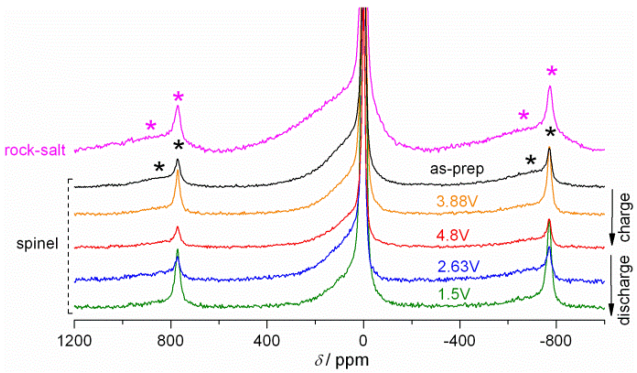

Fig. 5 ^{7}Li MAS NMR spectra of as-prepared $LiFeTiO_4$ and samples collected from the first cycle tested at room temperature. The ^{7}Li MAS NMR spectrum of the chemically synthesized rock-salt Li_2FeTiO_4 (top, pink line) is shown for comparison. Sidebands are marked with asterisks. A resonance at about 0 ppm originates from diamagnetic lithium species.

^{7}Li MAS NMR spectrum of the as-prepared $LiFeTiO_4$ shows a broad and asymmetric resonance line ranging from -100 to 300 ppm (Fig. 5), similar to the observation of Li^+ environment in other disordered spinel materials.[45] There is no indication of change in the local Li^+ environment upon first cycling. On charging to 4.8 V, a slightly noticeable reduction in intensity of the resonances was observed, indicating that certain Li^+ ions have been removed from the spinel host. Note that the Li^+ extraction out of $LiFeTiO_4$ is associated with the oxidation of Fe^{3+}. When the cell was discharged to 1.5 V, the resonance recovers in intensity and the initial spinel structure remains with a resulting Li-rich $Li_{1+y}FeTiO_4$. Chemically synthesized Li_2FeTiO_4 shows an even broader resonance line (-200 to 600 ppm) arising from the random cationic distribution in *Fm*-3*m* symmetry (Fig. 5). These results also confirm that there is no structural transition occurring due to Li^+ insertion.

The long-range order of the spinel lattice remains after extended cycling. Only reversible shifts in diffraction peak positions were observed (Fig. 6a, Fig. S3). $LiFeTiO_4$ shows minor lattice volume change over cycling, in comparison with the pristine host. A volume expansion of ~1.4% and a contraction of ~0.17% were observed (Table S3). The retention of the pristine spinel *Fd*-3*m* framework upon long-term cycling is responsible for its excellent cyclability. Such behaviour is attractive for durable energy storage systems. The stable host structure has been deemed as a major requisite for intercalation pseudocapacitance.[5] Although without structural change after 50 cycles, the cathodic peak located at 3.1 V from the CV curves becomes apparent. This suggests a slight change in the Li^+ insertion/extraction behaviour. Over cycling, the progressive increase in capacity and the change in lithiation voltage might be related to the minor structural rearrangement such as the change in Fe–O bond length and cationic displacement (Fig. S4).[46,47]

Several new diffraction peaks located at 2θ = 17.51°, 20.25° and 28.79° were observed after 160th charging (Fig. 6a), which can be indexed to *Fd*-3*m* symmetry (a = 8.044 Å). These results imply that extreme lithium extraction leads to a structural transition into two spinel phases. The newly formed spinel phase shows larger lattice contraction (10.7%, Table S3). Such behaviour has also been observed for spinel $LiMnTiO_4$,[21] $LiNi_{0.5}Mn_{1.5}O_4$[48] and $LiFe_{0.5}Mn_{1.5}O_4$.[49] The interfacial charge transfer reactions corresponding to the Li^+ insertion/extraction changed after long-term cycling, as probed by electrochemical impedance spectroscopy (Fig. S5). After 160 cycles at 40°C two well distinguished high-frequency semicircles were observed at 1.5 V, which might hint more than one interfacial charge-transfer process.

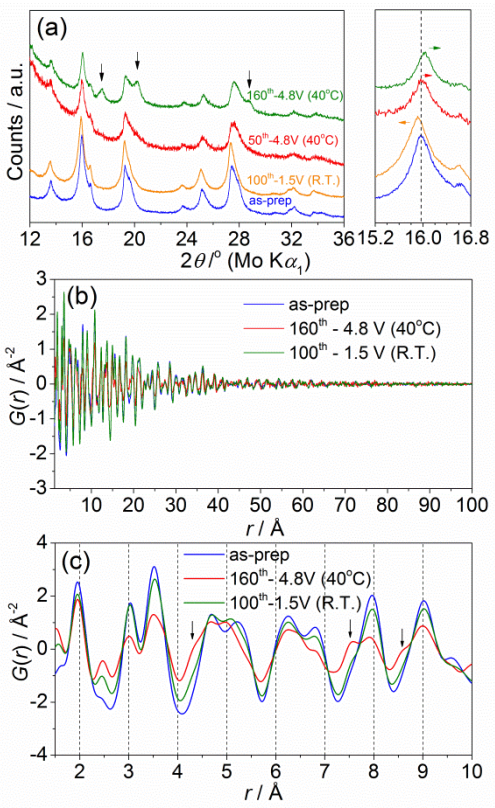

Fig. 6 (a) XRD patterns and (b,c) experimental PDF profiles for the as-prepared and cycled $LiFeTiO_4$/C. The vertical arrows mark the presence of a secondary cubic *Fd*-3*m* phase.

The features of the PDF profiles change only slightly after cycling (Fig. 6b,c), suggesting that the starting structure and the long-range order (up to ~50 Å, Fig. 6b) are retained. The PDF

curve of the fully discharged sample is nearly the same as that of the pristine material, indicating a minor structural change. For the fully charged sample, some different features can be observed after extended cycles with the presence of shoulders at shorter atomic distances as indicated by arrows in Fig. 6a. The positions of these peaks are close to the selected peaks corresponding to the Fe_{16d}–O, O–O and Fe_{8a}–O bonds as labelled in Fig. 1d. Thus, the observation is consistent with the XRD data that the presence of a new spinel phase is associated with unit cell contraction.[21] Furthermore, with the presence of the new phase, the ratio between the observed probabilities of the atom pairs changed due to the structural changes.

4. Conclusions

The combined XRD, NMR and PDF characterizations confirmed that the Li^+ is intercalated into nanoscale spinel $LiFeTiO_4$ with only minor changes in lattice parameter. Mössbauer spectroscopy verified that during Li^+ storage the oxidation state of iron changes reversibly in the bulk. The complete Fe^{3+}/Fe^{2+} redox reactions are involved and the partial Fe^{4+}/Fe^{3+} redox reactions are possible but not very conclusive. Thus, the Li^+ storage mechanism for $LiFeTiO_4$ is related to Li^+ intercalation into the lattice with the redox reactions of transition metal in the bulk, and the Li^+ intercalation kinetics is not solid-state diffusion limited. We conclude that the nanoscale $LiFeTiO_4$ exhibits intercalation pseudocapacitance Li^+ storage behaviour. In contrast to previous findings (metal oxides with well-defined microscopic architecture),[5,10,11] our work demonstrated for the first time that spinel $LiFeTiO_4$ as a model cathode material with nanoscale particle size enables intercalation pseudocapacitance Li^+ storage. It is believed that the spinel host allows the low energy diffusion path for Li^+. The unoccupied crystallographic sites are available for accommodating guest Li^+. Furthermore, the high-rate Li^+ storage in $LiFeTiO_4$ does not need advanced nanoarchitectures of electrode materials. More general solution routes can be used for material synthesis. The insights from this study shed light on designing high-rate Li^+ storage cathode materials for Li-ion batteries.

Acknowledgements

This work was financially supported by the BMBF and the "Helmholtz Initiative for Mobile/Stationary Energy Storage Systems". We acknowledge the synchrotron radiation source Petra-III (DESY) in Hamburg, Germany, for provision of beamtime at the P02.1 beamline.

Notes and references

[a] Institute of Nanotechnology, [b] Institute of Applied Materials, Karlsruhe Institute of Technology (KIT), P.O. Box 3640, 76021 Karlsruhe, Germany. E-mail: ruiyong.chen@kit.edu, sylvio.indris@kit.edu
[c] Helmholtz Institute Ulm for Electrochemical Energy Storage (HIU), 89081 Ulm, Germany
[d] Joint Research Laboratory Nanomaterials, Institute of Materials Science, TU Darmstadt, 64287 Darmstadt, Germany

Electronic Supplementary Information (ESI) available: additional electrochemistry and diffraction data. See DOI: 10.1039/b000000x/

1 B. Kang and G. Ceder, *Nature* 2009, **458**, 190.
2 P.G. Bruce, B. Scrosati and J.-M. Tarascon, *Angew. Chem. Int. Ed.* 2008, **47**, 2930.
3 S.W. Lee, N. Yabuuchi, B.M. Gallant, S. Chen, B.-S. Kim, P.T. Hammond and Y. Shao-Horn, *Nature Nanotech.* 2010, **5**, 531.
4 K. Brezesinski, J. Wang, J. Haetge, C. Reitz, S.O. Steinmueller, S.H. Tolbert, B.M. Smarsly, B. Dunn and T. Brezesinski, *J. Am. Chem. Soc.* 2010, **132**, 6982.
5 V. Augustyn, J. Come, M.A. Lowe, J.W. Kim, P.-L. Taberna, S.H. Tolbert, H.D. Abruña, P. Simon and B. Dunn, *Nature Mater.* 2013, **12**, 518.
6 A.A. Lubimtsev, P.R.C. Kent, B.G. Sumpter and P. Ganesh, *J. Mater. Chem. A* 2013, **1**, 14951.
7 P. Simon and Y. Gogotsi, *Nature Mater.* 2008, **7**, 845.
8 B.E. Conway, V. Birss and J. Wojtowicz, *J. Power Sources* 1997, **66**, 1.
9 R. Chen, V. Trieu, H. Natter, K. Stöwe, W.F. Maier, R. Hempelmann, A. Bulan, J. Kintrup and R. Weber, *Chem. Mater.* 2010, **22**, 6215.
10 T. Brezesinski, J. Wang, S.H. Tolbert and B. Dunn, *Nature Mater.* 2010, **9**, 146.
11 R. Giannuzzi, M. Manca, L. De Marco, M.R. Belviso, A. Cannavale, T. Sibillano, C. Giannini, P.D. Cozzoli and G. Gigli, *ACS Appl. Mater. Interfaces* 2014, **6**, 1933.
12 J.B. Goodenough and K.-S. Park, *J. Am. Chem. Soc.* 2013, **135**, 1167.
13 C. Lai, Y.Y. Dou, X. Li and X. P. Gao, *J. Power Sources* 2010, **195**, 3676.
14 M. Okubo, Y. Mizuno, H. Yamada, J. Kim, E. Hosono, H. Zhou, T. Kudo and I. Honma, *ACS Nano* 2010, **4**, 741.
15 J. Haetge, P. Hartmann, K. Brezesinski, J. Janek and T. Brezesinski, *Chem. Mater.* 2011, **23**, 4384.
16 J.M. Feckl, K. Fominykh, M. Döblinger, D. Fattakhova-Rohlfing and T. Bein, *Angew. Chem.* 2012, **124**, 7577.
17 A.D. Robertson, H. Tukamoto and J.T.S. Irvine, *J. Electrochem. Soc.* 1999, **146**, 3958.
18 Y. Sakai, K. Ariyoshi and T. Ohzuku, *Hyperfine Interact.* 2002, **139/140**, 67.
19 S.R. Bruno, C.K. Blakely and V.V. Poltavets, *ECS Trans.* 2012, **41**, 29.
20 J. Rodríguez-Carvajal, *Physica B* 1993, **192**, 55.
21 R. Chen, M. Knapp, M. Yavuz, R. Heinzmann, D. Wang, S. Ren, V. Trouillet, S. Lebedkin, S. Doyle, H. Hahn, H. Ehrenberg and S. Indris. *J. Phys. Chem. C.* 2014, **118**, 12608.
22 R. Chen, R. Heinzmann, S. Mangold, V.S.K. Chakravadhanula, H. Hahn and S. Indris, *J. Phys. Chem. C* 2013, **117**, 884.
23 S. Scharner, W. Weppner and P. Schmid-Beurmann, *J. Solid State Chem.* 1997, **134**, 170.
24 T. Tao, M.M. Rahman, T. Ramireddy, J. Sunarso, Y. Chen and A.M. Glushenkov, *RSC Adv.* 2014, **4**, 36649.
25 M. Sorescu, T. Xu, A. Wise, M. Díaz-Michelena and M.E. McHenry, *J. Magn. Magn. Mater.* 2012, **324**, 1453.
26 M.A. Arillo, M.L. López, E. Perez-Cappe, C. Pico and M.L. Veiga, *Solid State Ionics* 1998, **107**, 307.

27 N. Sharma, D. Yu, Y. Zhu, Y. Wu and V.K. Peterson, *Chem. Mater*. 2013, **25**, 754.
28 V. Petkov, *Mater. Today* 2008, **11**, 28.
29 B. Scrosati and J. Garche, *J. Power Sources* 2010, **195**, 2419.
30 D. Lv, W. Wen, X. Huang, J. Bai, J. Mi, S. Wu and Y. Yang, *J. Mater. Chem.* 2011, **21**, 9506.
31 P. Reale, S. Panero, F. Ronci, V. Rossi Albertini and B. Scrosati, *Chem. Mater*. 2003, **15**, 3437.
32 C. Kim, N.S. Norberg, C.T. Alexander, R. Kostecki and J. Cabana, *Adv. Funct. Mater*. 2013, **23**, 1214.
33 I.E. Rauda, V. Augustyn, B. Dunn and S.H. Tolbert, *Acc. Chem. Res.* 2013, **46**, 1113.
34 A.J. Bard and L.R. Faulkner, *Electrochemical Methods: Fundamentals and Applications* (Wiley, 1980).
35 G. Prado, A. Rougier, L. Fournès and C. Delmas, *J. Electrochem. Soc.* 2000, **147**, 2880.
36 Y. Takeda, K. Kanno, T. Takada, O. Yamamoto, M. Takano, N. Nakayama and Y. Bando, *J. Solid State Chem.* 1986, **63**, 237.
37 H. Shigemura, H. Sakaebe, H. Kageyama, H. Kobayashi, A.R. West, R. Kanno, S. Morimoto, S. Nasu and M. Tabuchi, *J. Electrochem. Soc.* 2001, **148**, A730.
38 J. Li, J. Li, J. Luo, L. Wang and X. He, *Int. J. Electrochem. Sci.* 2011, **6**, 1550.
39 D. Rangappa, K.D. Murukanahally, T. Tomai, A. Unemoto and I. Honma, *Nano Lett.* 2012, **12**, 1146.
40 M. Tabuchi, A. Nakashima, H. Shigemura, K. Ado, H. Kobayashi, H. Sakaebe, K. Tatsumi, H. Kageyama, T. Nakamura and R. Kanno, *J. Mater. Chem.* 2003, **13**, 1747.
41 A. Laumann, H. Boysen, M. Bremholm, K.T. Fehr, M. Hoelzel and M. Holzapfel, *Chem. Mater.* 2011, **23**, 2753.
42 L. Aldon, P. Kubiak, M. Womes, J.C. Jumas, J. Olivier-Fourcade, J.L. Tirado, J.I. Corredor and C.P. Vicente, *Chem. Mater*. 2004, **16**, 5721.
43 M. Küzma, R. Dominko, A. Meden, D. Makovec, M. Bele, J. Jamnik and M. Gaberšček, *J. Power Sources* 2009, **189**, 81.
44 R. Chen, M. Knapp, M. Yavuz and H. Hahn, *ECS Trans.* 2014, **61**, 19.
45 J. Cabana, M. Casas-Cabanas, F.O. Omenya, N.A. Chernova, D. Zeng, M.S. Whittingham and C.P. Grey, *Chem. Mater*. 2012, **24**, 2952.
46 K. Tateishi, D. du Boulay, N. Ishizawa and K. Kawamura, *J. Solid State Chem.* 2003, **174**, 175.
47 M. Wagemaker, F.G.B. Ooms, E.M. Kelder, J. Schoonman, G.J. Kearley and F.M. Mulder, *J. Am. Chem. Soc.* 2004, **126**, 13526.
48 R. Alcántara, M. Jaraba, P. Lavela and J.L Tirado, *Electrochim. Acta* 2002, **47**, 1829.
49 A. Bhaskar, N.N. Bramnik, D.M. Trots, H. Fuess and H. Ehrenberg, *J. Power Sources* 2012, **217**, 464.